The anisotropic seismic structure of the East European platform

Eric Matzel
Lawrence Livermore National Laboratory, Livermore, California, USA

Stephen P. Grand
Department of Geological Sciences, University of Texas at Austin, Austin, Texas, USA

Received 23 May 2001; revised 27 August 2003; accepted 25 September 2003; published 9 January 2004.

[1] We present models for the P and S velocity structure of the upper mantle beneath the East European platform including measurements of radial anisotropy. The models were obtained by full waveform inversion of 3-component broadband seismograms from strike-slip earthquakes located near the edge of the platform and recorded in Russia and Europe. We used direct and multiply reflected body wave arrivals (S, SS, P, PP) combined with fundamental mode Love and Rayleigh waves at source-receiver distances between 15° and 50° to resolve mantle structure down to the 410 km discontinuity. The platform is underlain by a radially anisotropic mantle lid extending to a depth of 200 km with a largely isotropic mantle below. The model has a positive velocity gradient from 41 km to 100 km depth, and a relatively uniform velocity structure from 100 km to 200 km depth with high SH and PH velocities (4.77 km/s, 8.45 km/s). Shear anisotropy is uniform at 5% ($\beta H > \beta V$) from 41 to 200 km depth, drops to 2% from 200 to 250 km and is isotropic below that. The average shear velocity from 100 to 250 km is also uniform at 4.65 km/s and the drop in anisotropy is matched by a drop in βH to 4.70 km/s combined with an increase in βV to 4.60 km/s. Below 250 km there is a positive velocity gradient in both P and S velocity down to 410 km. P anisotropy is not well resolved, but P structure mimics the SH velocity structure, suggesting that P is also anisotropic within the lid. *INDEX TERMS:* 8120 Tectonophysics: Dynamics of lithosphere and mantle—general; 8199 Tectonophysics: General or miscellaneous; 9335 Information Related to Geographic Region: Europe; 7218 Seismology: Lithosphere and upper mantle; *KEYWORDS:* anisotropy, inversion, mantle, Europe

Citation: Matzel, E., and S. P. Grand (2004), The anisotropic seismic structure of the East European platform, *J. Geophys. Res.*, *109*, B01302, doi:10.1029/2001JB000623.

1. Introduction

[2] Studies of the Earth's upper mantle have found a general relationship between the tectonic age of the crust and the velocity structure of the underlying mantle, with the highest velocities associated with the ancient cratons and the lowest velocities found beneath oceanic spreading centers and continental tectonic belts. Common features include the presence of a seismic high velocity region at the top of the mantle overlying a region of decreased velocities. These are referred to respectively as the seismic lid and low velocity zone (LVZ). The stable ancient cratons are typically underlain by deep high velocity root systems including fast seismic lids extending to 200 km or more. Phanerozoic regions have thinner lids and lower velocities and recently active regions have essentially no seismic lid and extremely low velocities. Beneath continents, velocity variations of several percent can extend down to the 410 km discontinuity or even deeper.

[3] The relationship between seismic velocity and tectonic age is most easily understood for oceanic regimes, where it appears to be directly related to the thickening of the lithosphere as the plate cools. Velocities are slowest directly beneath the spreading ridges and increase rapidly with the age of the plate. The increase in velocity occurs first in the shallowest portion of the plate and propagates down over time resulting in the formation of a fast seismic lid over a LVZ [*Forsyth*, 1975; *Leeds*, 1975; *Regan and Anderson*, 1984; *Gaherty et al.*, 1999; *Xu and Wiens*, 1997; *Grand and Helmberger*, 1984b; *Zhao and Helmberger*, 1993]. Most of the lateral heterogeneity in the oceanic mantle is due to the variations in lid thickness and velocity. The mantle below the lid is much more homogeneous, suggesting that it is free to mix over geologic timescales. Together, these observations suggest that the lid represents both a thermal and mechanical boundary layer. The thickening lid is believed to be the lithosphere and the underlying LVZ is thought to be a zone of partial melting.

[4] Beneath continents the situation is more complicated. The general relationship of higher velocities under older regimes still holds, but there is more variability between provinces of similar age [*Simons et al.*, 2002]. As in oceanic regions, the seismic lid is associated with the thermal state of the mantle. The lid is thickest beneath the cold, stable cratons, reaching 200–250 km depth. There is virtually no

0148-0227/04/2001JB000623$09.00

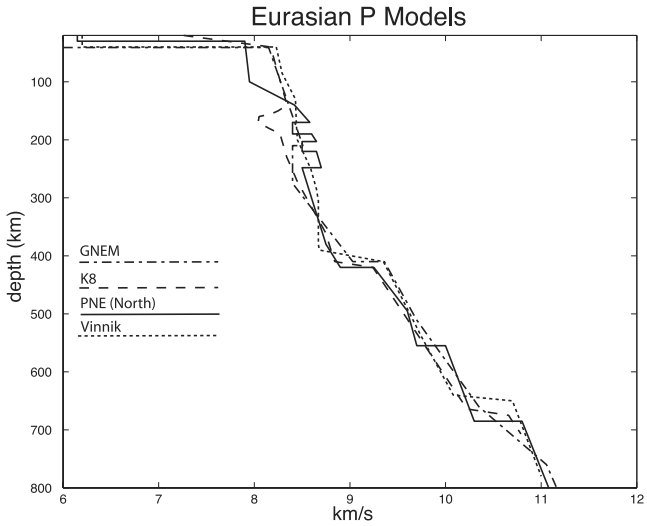

Figure 1. A comparison of several P models for Eurasia. GNEM [*Ryberg et al.*, 1995], PNE North [*Mechie et al.*, 1993], and Vinnik [*Vinnik and Ryaboy*, 1981] were obtained using data from the Peaceful Nuclear Explosions experiment conducted in the Soviet Union. K8 [*Given and Helmberger*, 1980] used earthquake sources.

lid beneath active, tectonic areas [*Grand and Helmberger*, 1984a; *Walck*, 1984]. Unlike the oceanic case, however, there are large variations in mantle velocity below the lid, suggesting that the thermal and mechanical boundary layers are decoupled. Deep roots of high P and S velocity lie beneath the Archaen cratons and extend well below the mantle lid [*Given and Helmberger*, 1980; *Grand and Helmberger*, 1984a; *Paulssen*, 1987; *Lefevre and Helmberger*, 1989; *Vinnik et al.*, 1996; *Qiu et al.*, 1996; *Priestley*, 1999]. This suggests that the tectonic plates may reach hundreds of kilometers in thickness in places. *Jordan* [1988] refers to the region of the Earth that moves coherently during plate tectonics as the tectosphere. He interprets the deep cratonic roots as evidence that cratons are compositionally distinct from the surrounding mantle, allowing them to remain stable on geologic timescales. *Anderson* [1995] points out that another interpretation is that the roots represent cold mantle downwellings. Estimates for the lower boundary of the tectosphere beneath cratons range between 150 and 410 km depth [*Gaherty et al.*, 1999; *Li et al.*, 1998; *Jordan*, 1988]. Low velocity zones at ~150–200 km are common in several models [*Pavlenkova et al.*, 1996; *Qiu et al.*, 1996; *Lefevre and Helmberger*, 1989; *Grand and Helmberger*, 1984; *Given and Helmberger*, 1980], but absent or very deep in others [*Gaherty et al.*, 1999; *Zhao et al.*, 1999; *Vinnik et al.*, 1996]. This may be a fundamental difference between cratons or a consequence of the different methods, assumptions and types of data used to determine the seismic structure.

[5] The structure of both P and S velocity models shows heterogeneity in the upper several hundred kilometers, related to tectonic regime. The details differ, however, and questions remain about how to relate the two. In particular, LVZ's are more consistently found in S models than in P models, and often vary in thickness and location when found in both. Part of the problem is that most studies still model either S or P structure only, and differences in the data and methodology used make direct comparison of the structures difficult. The relationship between S and P velocity is important, because a drop in S velocity without a corresponding drop in P velocity may indicate the presence of partial melt. That is the interpretation of *Rodgers and Bhattacharyya* [2001] who modeled both P and S structure for the central U.S. and found a shear LVZ, but none for P. *Qiu et al.* [1996] found a similar relationship for the P and S structure of southern Africa. However,

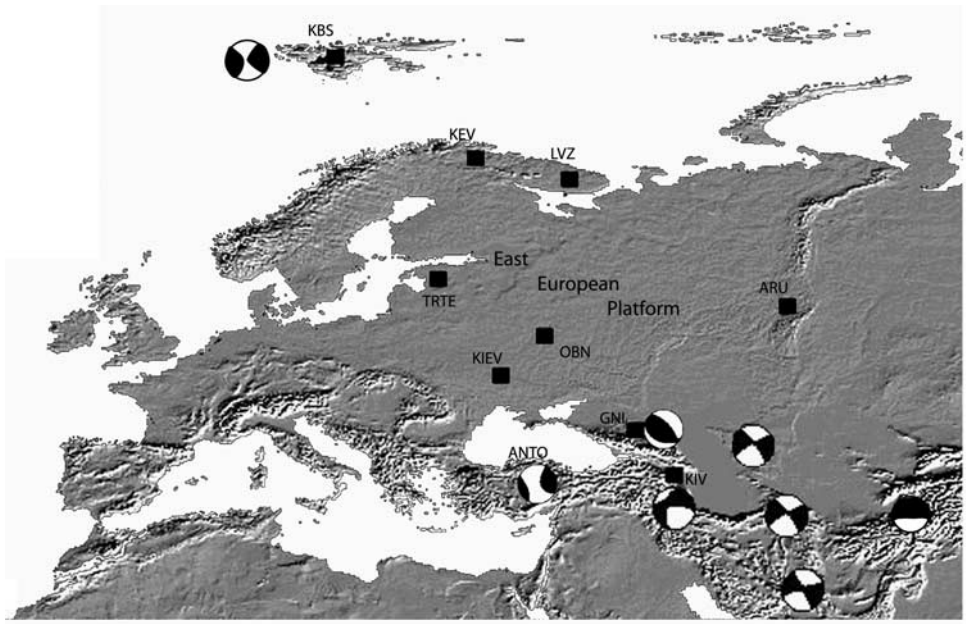

Figure 2. A map of the study area including the earthquake sources (beachball figures) and seismic stations (squares) used. The East European platform includes most of Russia west of the Urals.

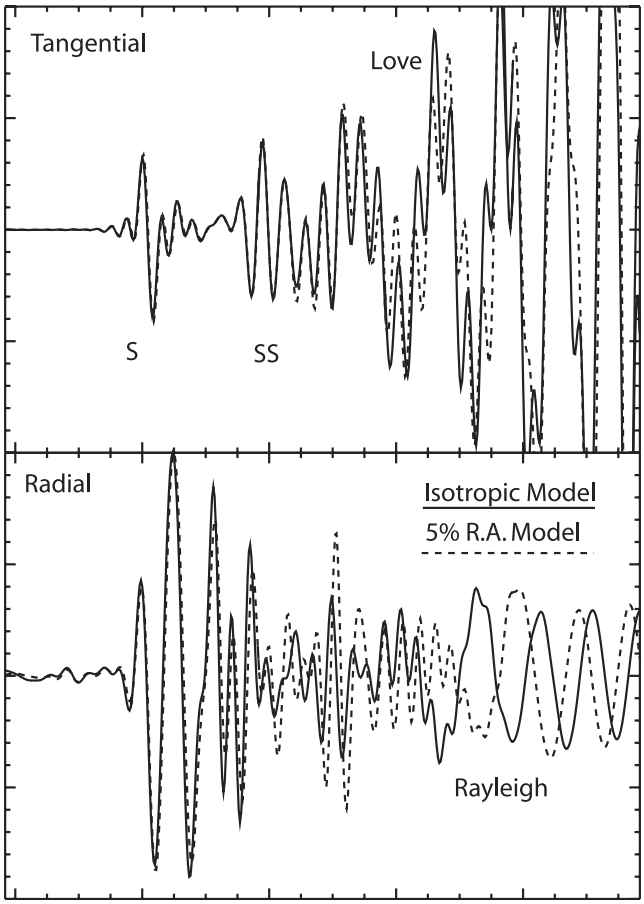

Figure 3. Sensitivity of data to anisotropic structure. Tangential and radial component synthetics are plotted for an isotropic model (solid line) and a radially anisotropic model (dashed line). Major arrivals are identified for reference. Both models (isotropic and anisotropic) have the same SH structure. In the anisotropic model, βV is 5% slower than βH from the Moho to 200 km depth. The anisotropic radial component arrivals (both body and surface waves) are delayed relative to the isotropic synthetics. The tangential component synthetics show little sensitivity to anisotropy, except for the most steeply incident body wave arrivals.

Gaherty et al. [1999] identified both a P and S LVZ beneath Australia related to the transition from anisotropic to isotropic mantle.

[6] Some of the most detailed P velocity models were obtained using data from the Peaceful Nuclear Explosions (PNE) experiment conducted in the 1970s and 1980s in the Soviet Union. In those experiments, 3-component short period P wave data were collected for long-range profiles covering much of the Siberian and Russian platforms. The 1-D and 2-D models of these profiles, which have been developed to investigate the structure of the upper mantle and transition zone, indicate significant vertical and lateral heterogeneity throughout the region (Figure 1) [*Mechie et al.*, 1993; *Morozova et al.*, 1999; *Pavlenkova and Yegorkin*, 1983; *Ryberg et al.*, 1995, 1998; *Vinnik and Ryaboy*, 1981]. The heterogeneity of the upper 100 km correlates well with heat flow measurements and the age of different tectonic units, with slower velocities associated with younger regions [*Pavlenkova and Yegorkin*, 1983]. The observation of a teleseismic Pn phase followed by a long noisy coda has been interpreted as evidence that the shallowest mantle consists of a zone of small randomly distributed scatterers which serve as a waveguide [*Ryberg et al.*, 1995]. These observations suggest that the zone extends to at most 100 km depth, below which there is a fundamental change in either the scale of the heterogeneity, or the value of seismic attenuation, Q. It is also notable that the depth, sharpness and magnitude of the transition zone discontinuities vary markedly from one model to the next. This may reflect real differences in structure along the different profiles, or may

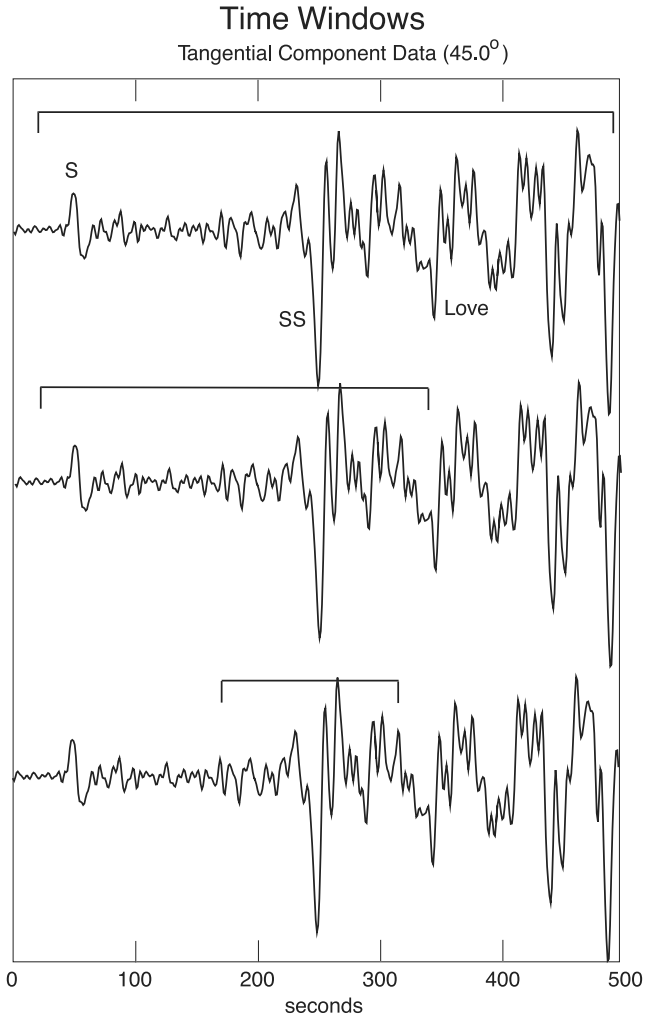

Figure 4. An example of time windows used in the inversion procedure. The traces are the tangential component data at 45°. The first arrival is the direct S phase. The black lines indicate the portion of the data that was inverted in 3 different runs. In the first run the entire seismogram was inverted, beginning with the direct S arrival through the surface wave arrivals (top). Inclusion of the surface waves provides good resolution of the shallowest structure. Subsequent runs were inverted starting from the that result, but focusing on narrower portions of the data and solving for finer-scale structure at depth (middle, bottom).

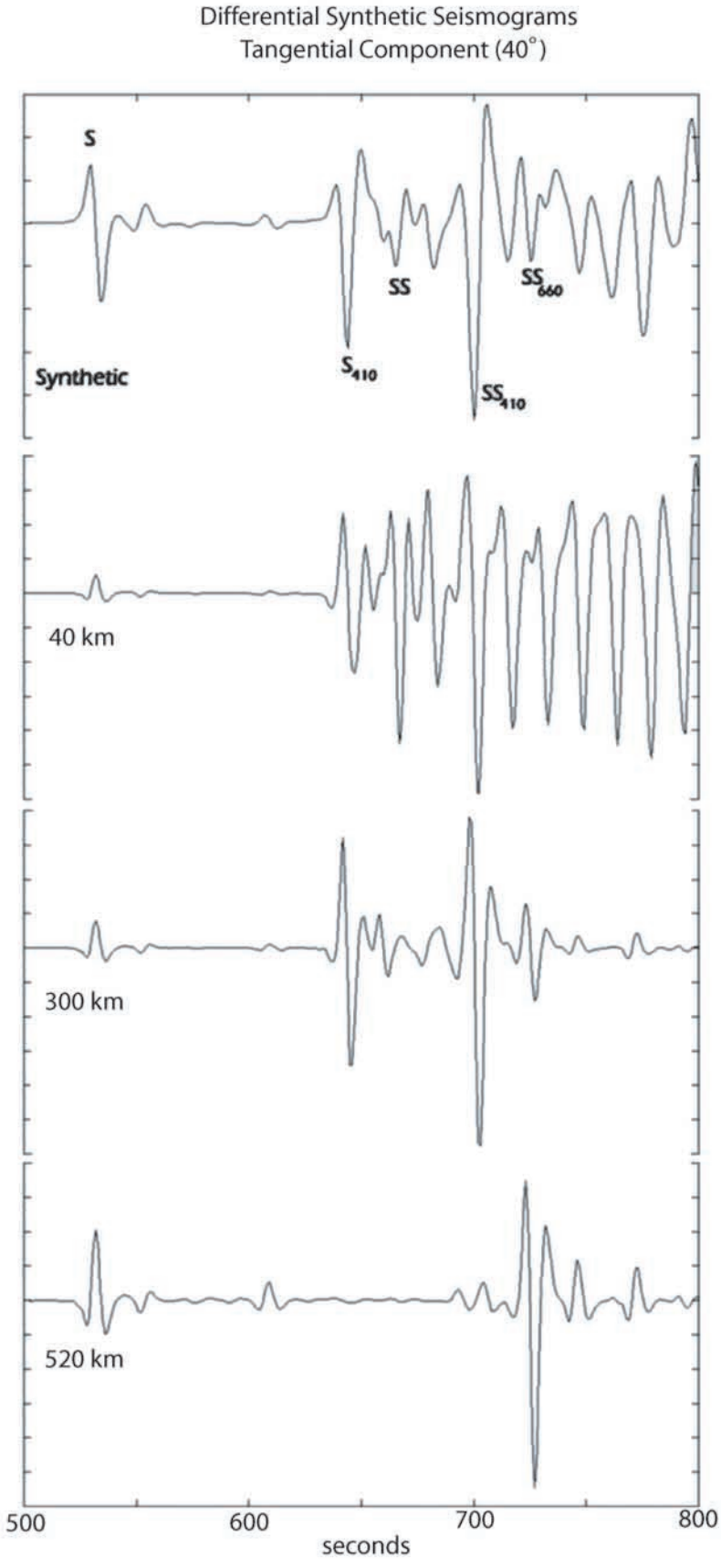
Differential Synthetic Seismograms
Tangential Component (40°)
S
SS
SS660
S410
SS410
Synthetic
40 km
300 km
520 km
500
600
700
800
seconds

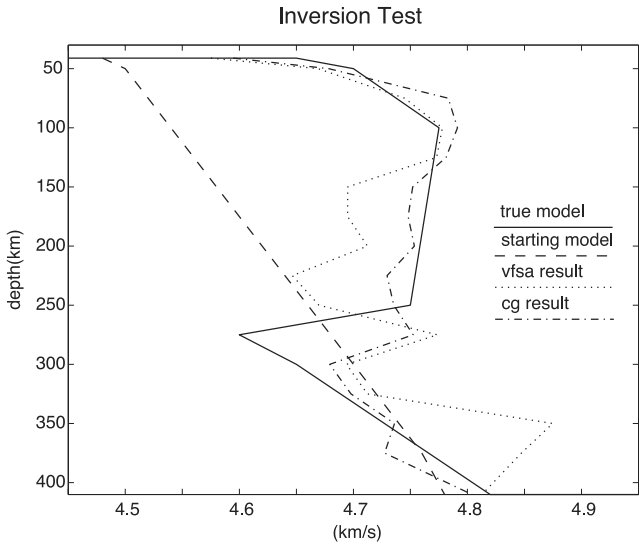

Figure 6. A test of the waveform inversion procedure. Synthetic seismograms were created for an isotropic SH velocity model (solid line) and used as the data in an inversion test. The inversion was begun using a simple starting model with positive velocity gradient from the Moho down to the 410 km discontinuity (dashed line). The inversion was initially run for 100 iterations using the VFSA method (dotted line). That result was then used as the starting point for the CG inversion. The CG result converges after 7 iterations (dashed-dotted line).

be the result of the different methods used. Among the common features of these models is a distinct LVZ at around 200–300 km, similar to the depth range often found in shear wave studies of continental regimes. Unfortunately, due to the nature of the sources involved, there was no complimentary S wave data to use for comparison.

[7] The purpose of this work is to develop a seismic inversion procedure to produce simultaneous P and S velocity models of the upper mantle and to apply that procedure to investigate the seismic structure of the upper mantle beneath the East European platform (EEP). The inversion was designed to match both timing and amplitude information of the body and surface wave arrivals in the data. Variables in the inversion include the five elastic constants that determine the seismic velocities in a radially anisotropic medium. Synthetic seismograms are compared to data to evaluate the fit of the models. Differential synthetic seismograms determine the influence of each model variable on the resulting synthetics. The full waveform from the start of the first body wave through the surface waves is used in the evaluation. All three components of the data (vertical, radial and tangential) are used in order to provide coincident information for the horizontally and vertically polarized components of α and β.

[8] This study focuses on the seismic structure of the East European platform, a Precambrian age structure that comprises most of Russia west of the Urals (Figure 2) that has remained relatively undeformed since 1.6 Ga. [*Glebovitsky*, 1997; *Zonenshain et al.*, 1990]. This area has been studied in part by several groups [*Marquering and Snieder*, 1996; *Zielhuis and Nolet*, 1994; *Vinnik and Ryaboy*, 1981; *Ryberg et al.*, 1995; *Paulssen et al.*, 1999; *Muyzert et al.*, 1999]. P wave structure appears particularly heterogeneous in the upper 100 km. *Vinnik and Ryaboy* [1981] identify a low velocity layer between 60–110 km, while *Ryberg et al.* [1995] used observations of teleseismic Pn to propose a zone of elongated scatterers from the base of the crust to 100 km depth. *Marquering and Snieder* [1996] found a relatively laterally homogenous, fast S wave velocity structure beneath the platform extending to 300 km depth. This is also apparent in the 2-D profile from the NARS experiment which shows a sharp transition in the thickness of the lithospheric root between the EEP (200 km) and younger continental regions (100 km) [*Muyzert et al.*, 1999; *Paulssen et al.*, 1999].

2. Seismic Anisotropy in the Earth's Mantle

[9] In an anisotropic medium, elastic properties vary as a function of direction and polarization. Anisotropy is an inherent feature in most minerals and mineral assemblages found in the upper mantle [*Hess*, 1964; *Kern*, 1993; *Nicolas and Christensen*, 1987]. Anisotropy tends to average out over the large scale if individual crystals are oriented randomly; however, if they are aligned, the medium as a whole can become anisotropic.

[10] Many seismic studies have concluded that the upper mantle is highly anisotropic, but the location, extent and magnitude of this anisotropy are uncertain [*Ekstrom and Dziewonski*, 1998; *Montagner and Tanimoto*, 1991; *Gaherty and Jordan*, 1995]. Anisotropy is often represented as a radially anisotropic layer with several percent differences between the vertical and horizontal seismic speeds. It is typically observed by measuring the mismatch of Love and Rayleigh waves, or by a mismatch in the arrival times of body wave phases such as SH and SV [*Gaherty et al.*, 1999]. Figure 3 illustrates the effect of anisotropy on the tangential (SH) and radial (SV) components of teleseismic data. Fundamental mode surface wave measurements have poor resolution below ~200 km depth, and measurements of anisotropy from body wave phases integrate the effects of anisotropy along the path length. Travel paths that pass through different tectonic regions of the mantle also often complicate the data.

[11] An inherently isotropic medium with heterogeneity on scales smaller than a seismic wavelength can generate anisotropic effects. For instance, small-scale scatterers or a series of thin layers with sharp velocity contrasts can result in anisotropic propagation of seismic waves. *Backus* [1962]

Figure 5. An example of the use of differential synthetic seismograms. Plotted are the tangential component synthetic and 3 differentials for a source receiver offset of 40°. The top trace is a full synthetic seismogram for a starting model with major phases identified. The remaining 3 traces are differentials produced by subtracting synthetics of perturbed models from the original synthetic. In each case the S velocity of a single layer has been perturbed by 0.1% from the original model. The layers were located at 40–60 km depth; 300–320 km depth and 520–540 km depth respectively.

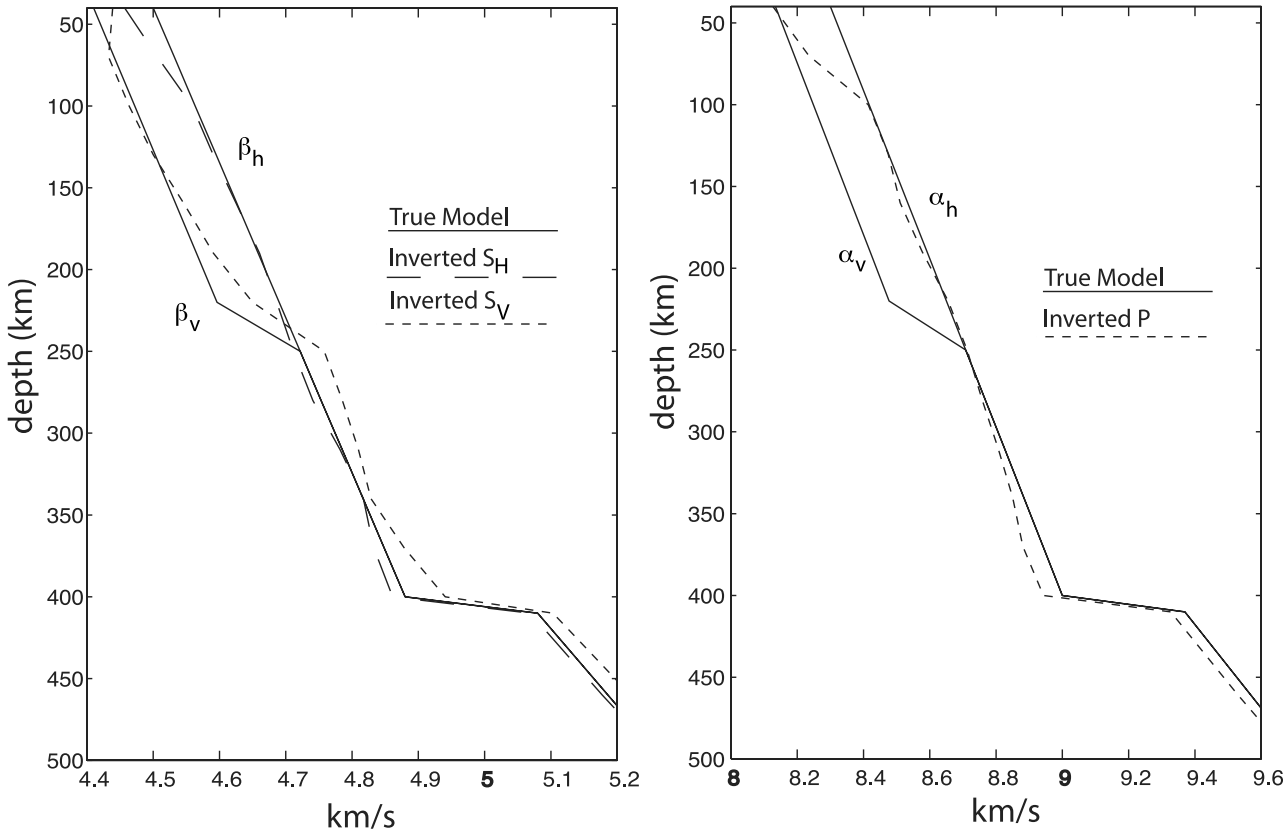

Figure 7. Inversion of anisotropic data using an isotropic assumption. 3 component synthetic seismograms were created for a model with α% and β% = 2% ($\beta V < \beta H$; $\alpha V < \alpha H$; $\eta = 0.90$) from the Moho to 220 km (solid lines). These were used as data in separate inversions of βSH and βSV and α using an isotropic assumption. The results of the inversions are shown (dashed lines).

illustrated this point by proving that radial anisotropy is equivalent to fine horizontal stratification. *Ryberg et al.* [1995] proposed an earth model containing small-scale horizontally elongated scatterers extending to 100 km depth beneath northern Eurasia to explain the Pn coda on short period seismograms and such a structure could also produce anisotropic phenomena. Additionally, *Saltzer et al.* [2000] argue that a stack of azimuthally anisotropic layers, with different fast axis orientations may average out the azimuthal component of anisotropy, but the radially anisotropic component could be preserved. *Rumpker et al.* [1999] disagree, however, concluding that a $\pi/2$ periodicity with respect to backazimuth will result.

[12] Seismic anisotropy in the upper mantle is typically attributed to the alignment of olivine due to tectonic forces [*Artyushkov*, 1984; *Anderson*, 1989]. This implies that measurements of anisotropy are directly related to mantle flow and deformation. A critical element desired in analyses of seismic anisotropy is an explicit demonstration of the location and depth extent of the anisotropy. This is important because anisotropy can be a result of relict flow frozen into the lithosphere, active deformation in the asthenosphere or a combination of both. In the first case it represents an historical record of tectonism, in the second it is a picture of present-day convection.

[13] It is also important to consider anisotropy when comparing different seismic models. S models, for instance,

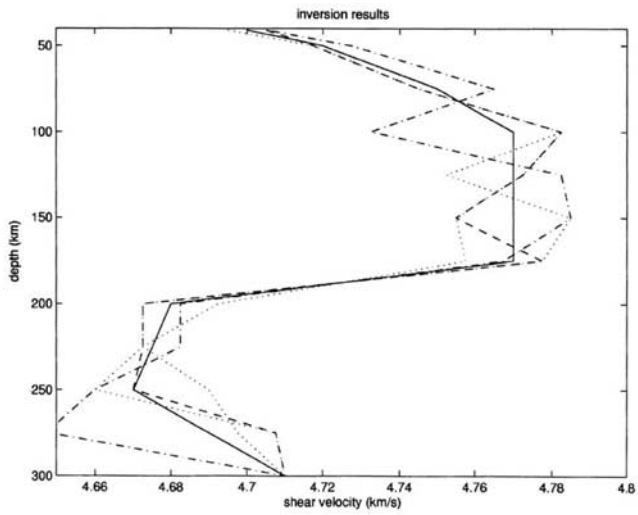

Figure 8. A series of inversion results for the same data set (dashed lines). The inversion was run several times using different starting models. The final result (solid line) is a smoothed version produced by averaging the inversion runs. Synthetic seismograms for all of these models are virtually indistinguishable at the frequencies used in the study.

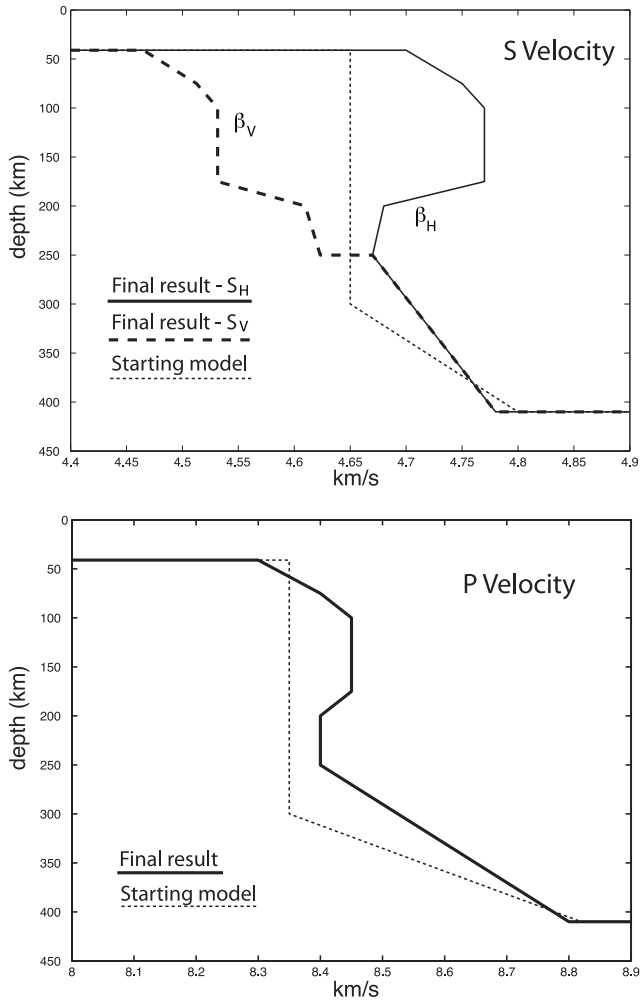

Figure 9. The starting and final models for the East European platform data set. The inversion was begun with an isotropic earth model with a homogeneous velocity structure from the Moho to 300 km. Shear wave radial anisotropy ($\beta V < \beta H$) is required to match the data. P anisotropy is unresolved.

often focus on either the radial component (SV) or tangential component (SH) of the data. When comparisons are made between such data sets, variations may be interpreted as fundamental differences in Earth structure. If the subsurface is isotropic this is justified, but if it is anisotropic it is not. Neglecting anisotropy can also bias isotropic models because the velocity of a ray through an anisotropic medium is a function of incidence angle [*Regan and Anderson*, 1984; *Laske and Masters*, 1998; *Simons et al.*, 2002].

3. Data

[14] Seismic data provide a great deal of information about the Earth's interior. Seismograms can contain direct and multiply reflected arrivals, converted phases and surface waves. The data are complicated by the large number of arrivals present, and can be difficult to interpret. In addition, the 3 components of each seismogram (vertical, radial and tangential) are sensitive to different phases. The tangential component isolates purely SH motion and contains only S body phases and Love waves and has been used extensively to obtain S wave structure in the Earth. The radial and vertical components contain both P and SV components including the Rayleigh waves. Fundamental mode Love and Rayleigh surface waves provide some of the best constraints on the shallow part of the mantle (less than ~200 km depth). Body wave arrivals are more sensitive to deeper structure. We use the full waveform, from the start of the first body wave through the surface waves, to obtain 1-D models of P and S structure including an analysis of radial anisotropy.

[15] The data used in this study are 3-component broadband seismograms from 8 moderate magnitude (5.5–6.5 Mb), earthquakes located near the East European platform and recorded in Russia and Europe (Figure 2). The data were selected based on several criteria: First, most of the source-receiver path had to fall within the EEP. This required selecting sources and receivers within the platform or as close to it as possible. Second, we wanted moderate magnitude events, with simple source time functions and good signal-to-noise ratios. Finally, we wanted data with identifiable P and S arrivals so that we could create a coupled P and S velocity model.

[16] We chose source-receiver combinations at offsets between 10° and 50° because they include identifiable direct arrivals, multiple arrivals and surface waves that can be used to resolve structure at various depths in the upper mantle. A total of 45 seismograms from the 8 sources make up the data set. Direct (S, P) and multiply reflected (SS, PP) arrivals, converted phases and surface waves are all readily identifiable on the seismograms and provide very good resolution of the upper mantle radial structure.

[17] A significant problem for our study of the EEP is the limited number of available seismic stations. Our requirement that the source-receiver paths predominantly sample the platform results in a NW-SE bias in the path coverage. Most of the seismicity occurs to the south of the platform and most of the available stations are located to the north and west of those sources. ARU is the only station near the eastern edge of the platform and source-receiver offsets to ARU fall between 18°–28°. Our only northern event (3/21/1998) is located within 216 km of our northernmost station, KBS, and the source-receiver paths sampling the platform also fall along a NW-SE arc. This bias in path coverage

Table 1. Seismic Model for the East European Platform

z, km	αH, km/s	βH, km/s	βV, km/s	η
0.0	2.50	1.10	1.10	1
0.5	4.00	2.10	2.10	1
2.0	6.20	3.60	3.60	1
17.0	6.20	3.60	3.60	1
32.0	6.60	3.70	3.70	1
41.0	7.30	4.00	4.00	1
41.1	8.30	4.70	4.47	0.95
75.0	8.40	4.75	4.51	0.95
100.0	8.45	4.77	4.53	0.95
175.0	8.45	4.77	4.53	0.95
200.0	8.40	4.68	4.62	0.97
250.0	8.40	4.67	4.63	0.97
250.0	8.40	4.67	4.67	1
410.0	8.80	4.80	4.80	1

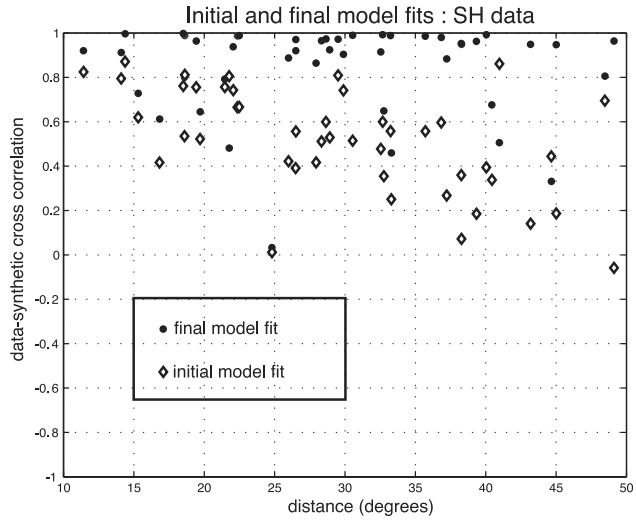

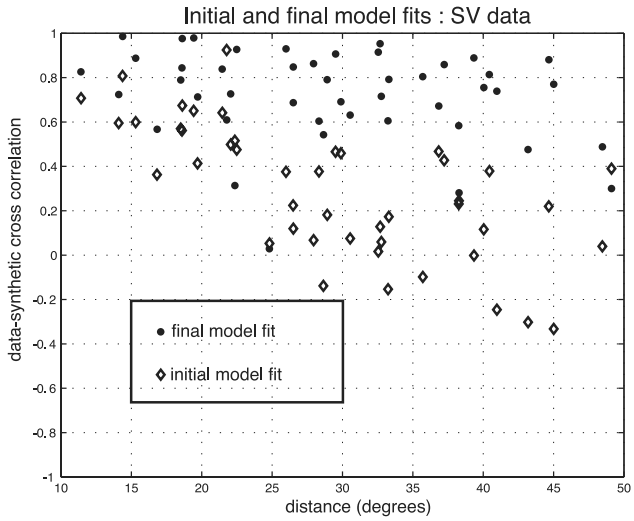

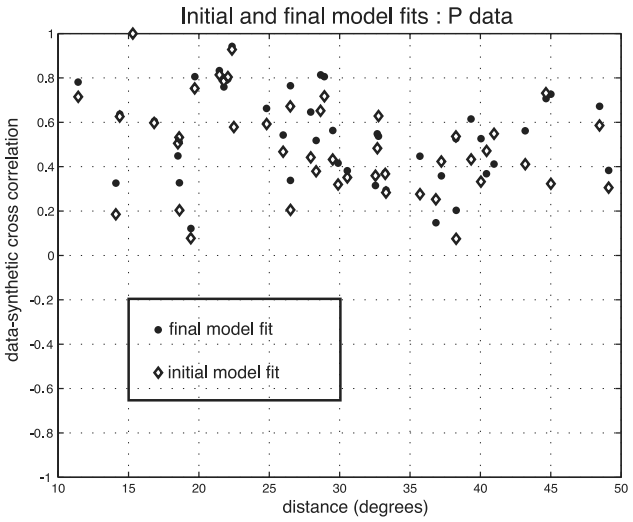

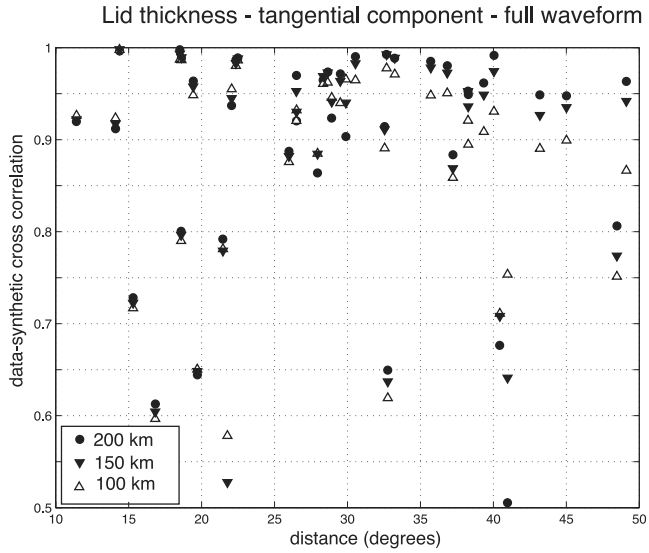

Figure 11. A test of the thickness of the seismic lid, focusing on surface waves. The cross correlations between tangential component data and synthetic seismograms for models with lids extending to 100 (open triangles), 150 (filled triangles), and 200 km depth (circles), respectively.

means that azimuthal anisotropy is poorly resolved and that our results might best be interpreted as valid for a corridor within the platform rather than for the platform as a whole. Because of the limited data set, we proceeded with two assumptions: first, that the platform can be generally described by a 1-D radially anisotropic structure and second, that azimuthal anisotropy in the platform is small or averages out over the path lengths involved. The assumption of lateral homogeneity is supported by the results of *Marquering and Snieder* [1996] and 2D profiles of *Paulssen et al.* [1999]. *Vinnik and Ryaboy* [1981] found that the average upper mantle azimuthal anisotropy in the platform does not exceed 0.5%.

4. Inversion Method

[18] We have developed a procedure for the efficient inversion of seismic waveforms to produce models of the Earth's mantle structure. Our technique is an iterative, nonlinear method combining the advantages of simulated annealing and least squares gradient techniques [*Sen and Stoffa*, 1995; *Tarantola*, 1984; *Mora*, 1988]. The variables in the problem are the seismic velocities (α and β) and the density (ρ) as a function of depth. When transverse isotropy is required this set is expanded to include the five variables

Figure 10. The cross-correlation between data and model synthetics for the initial (diamonds) and final (circles) models. The tangential component, SH (top), and radial component, SV (middle) correlation windows included phases from the first S arrival through the fundamental mode surface waves. The vertical component, P (bottom) correlation window included only phases between the direct and multiple P arrivals. The frequency band was between 0.01–0.05 Hz.

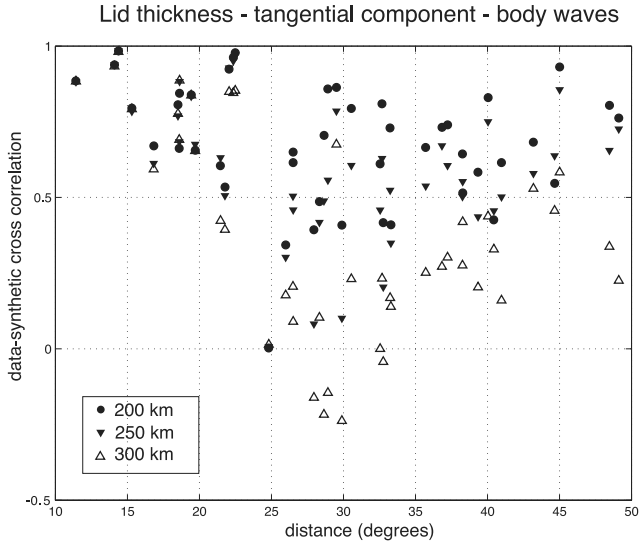

Figure 12. A test of the thickness of the seismic lid, focusing on body waves. The cross correlations between tangential component data and synthetic seismograms for models with lids extending to 200 (circles), 250 (filled triangles) and 300 km (open triangles), respectively.

that determine the seismic velocities in a transversely isotropic medium (αH, αV, βH, βV, η).

[19] Several factors complicate the inversion of seismic data: The equations involved are nonlinear, the size of the problem is very large, and the solutions obtained are not unique. Addressing the non-linearity and uniqueness problems requires extracting as much information as possible from the data and also requires using information known independently of the data to place physically realistic bounds on the solution. *Tarantola* [1984] has shown that using the entire seismogram, including amplitude and timing information, increases the stability of the problem and dramatically reduces the uncertainty of the solution. In this study, we used the full waveform, from the start of the first body wave through the surface waves, in the evaluation. All 3 components of the data (vertical, radial and tangential) were used in order to resolve the horizontally and vertically polarized components of α and β.

[20] To take advantage of the full waveform, a method for calculating complete and accurate synthetic seismograms is required. In this study, synthetic waveforms for isotropic and transversely isotropic models were created using the reflectivity technique [*Fuchs and Muller*, 1971; *Randall*, 1994]. This method provides synthetic seismograms for 1-dimensional Earth models with accurate frequency, timing and amplitude characteristics of all phases, including the surface waves, which can be compared directly to the recorded data. Radially anisotropic structures were created using the fine-layered equivalency equations of *Backus* [1962].

[21] To be useful, the inversion must be both accurate and efficient. The number of variables, the time required to calculate each iteration and the number of iterations control the efficiency of the method. To address this problem we inverted the data in several steps over a number of frequency windows as described by *Nolet et al.* [1986]. Frequency window techniques have been used successfully to obtain crustal models from seismic reflection data [*Pica et al.*, 1990] and to obtain models of the upper mantle [*Xu and Wiens*, 1997]. The procedure begins by filtering the data over a narrow band focused on low frequencies, inverting to get an initial model, then increasing the bandwidth and inverting again using the previous result as a starting model. This process is repeated until the full bandwidth is used. In this study, the data were initially band-pass filtered between 5–20 mHz (200–50 s period) and inverted for the large-scale radial structure of the model. In subsequent steps, the high-pass corner of the filter was progressively increased to a maximum of 100 mHz (10 s period) and the model was inverted for finer-scale structures.

[22] Frequency window techniques have two notable advantages for our study. The first is that the sensitivity of seismic data to the Earth's structure changes depending on the frequency band that is observed. The lower frequency portions of the data are most sensitive to the long wavelength variations in velocity, while high frequency bands are most sensitive to strong gradients. The low frequency result is therefore a good low-resolution model and the higher frequency steps can be regarded as more finely detailed perturbations of that model. The second advantage is that the speed of the reflectivity method is directly related to the range of frequencies used, so the initial narrow-band steps proceed relatively quickly.

[23] In addition to using frequency windows, we also employ time windows in our inversion scheme. Time windows are the portion of each seismogram which the inversion tries to duplicate with synthetics. Initially, we select the entire seismogram from the first body wave arrival through the surface wave and the inversion attempts to match the entire waveform. In subsequent steps, we progressively reduce the time-window and focus on specific arrivals (Figure 4). This procedure results in a top-down solution for the Earth model, fitting the data most sensitive to shallow structure first and progressively solving for deeper structure, and it prevents the larger surface wave arrivals from dominating the final inversion result.

[24] Seismic inversion methods often involve the minimization of a function that describes the misfit between the observed data and model synthetics. Various methods have been developed to minimize the misfit. Random walk methods are good at finding the global minimum, but require a prohibitive number of iterations to converge when a high resolution model is desired. Gradient methods achieve rapid convergence by calculating the best 'next step' in the inversion, but can get trapped in a local minimum. We have combined the advantages of these methods to achieve quick convergence to the global best fit model.

[25] This inversion employs a normalized cross-correlation misfit function. Data are directly compared to synthetics to establish a match. The initial data vectors (d0) are the seismic waveforms recorded at each station. Synthetic seismograms make up the other data vectors (dn). The cross correlation is performed over the time window specified at the start of the inversion. The fit of the model is established by the cross-correlation between the data and synthetics normalized by their autocorrelations.

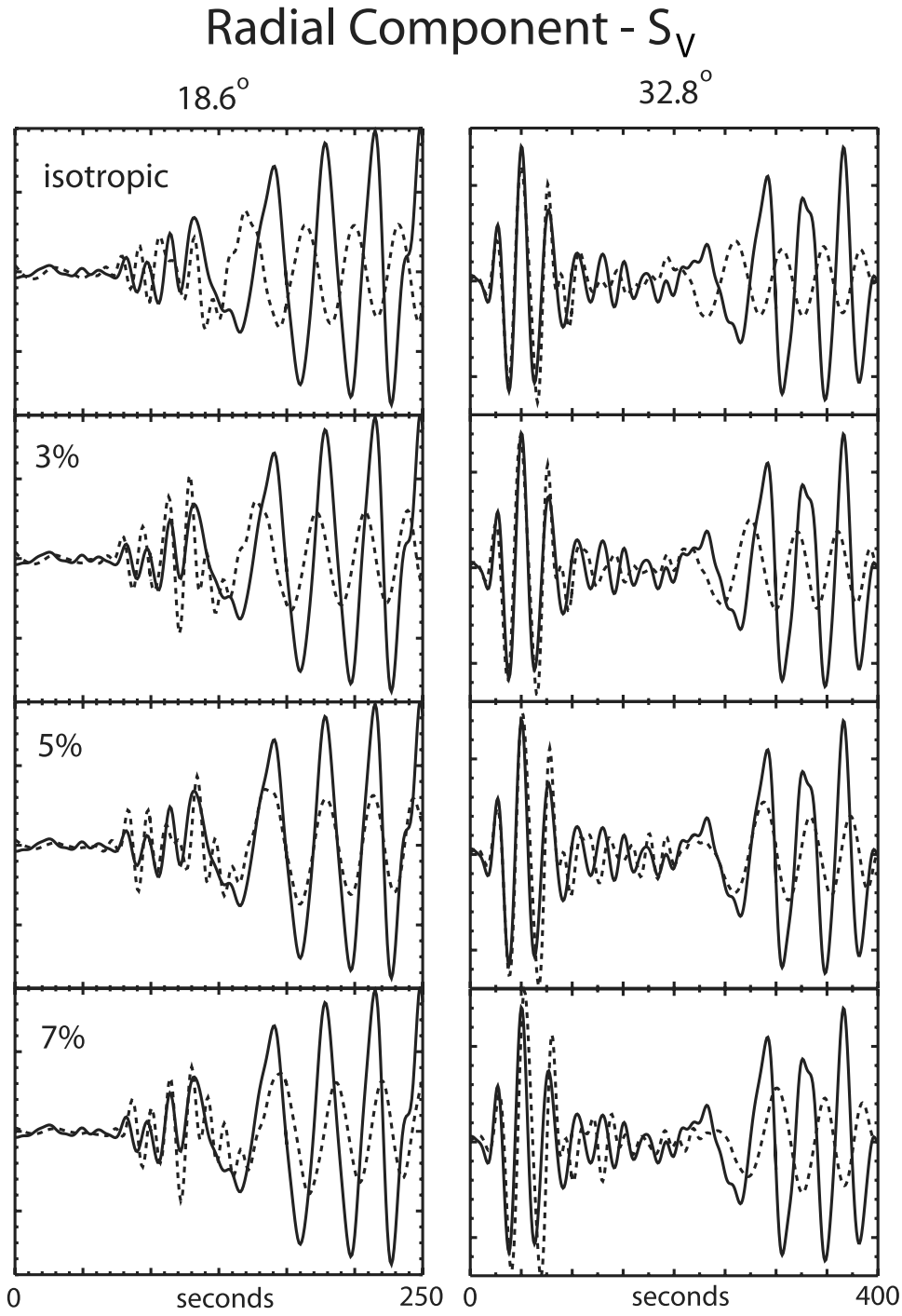

Figure 13. Evidence for anisotropy in the mantle lid: radial component synthetics for isotropic and radially anisotropic models (dashed) are compared with data (solid) for two of the stations used in this study. The first arrival is the direct S wave, SS and Rayleigh waves are also evident. Synthetics were calculated using a constant SH model and anisotropy was calculated relative to that. The top traces are for isotropic models, below that are traces for models with 3%, 5% and 7% radial anisotropy ($\beta V < \beta H$). In these models the anisotropy is uniform throughout the lid. Below the lid the models are isotropic.

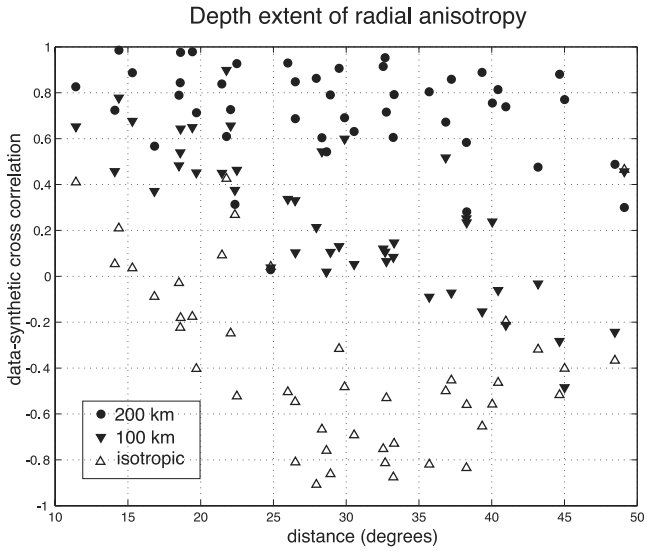

Figure 14. A test of the depth extent of radial anisotropy, focusing on Rayleigh waves. The cross correlations between radial component data and synthetic seismograms for an isotropic model (open triangles) and models with 5% anisotropy extending to 100 (filled triangles), and 200 km (circles).

xc z= correlation(d0,dn)
ac z= correlation(d0,d0)
sc z= correlation(dn,dn)
S z= 1 − (xc/sqrt(ac*sc))

[26] The specific procedures we use are the very fast simulated annealing (VFSA) method [*Sen and Stoffa*, 1995] and the conjugate-gradient (CG) method [*Mora*, 1988].

5. The Very Fast Simulated Annealing Inversion Method (VFSA)

[27] VFSA is a random walk procedure that has been optimized to speed convergence [*Sen and Stoffa*, 1995]. The optimization is accomplished using a probability function (T) that governs both the step size and the acceptance criteria. T is referred to as the "temperature" function due to the heat-bath analogy used in developing VFSA. After each iteration, the variables in the model are perturbed relative to the "best fit" model. The step size is the change in each model variable from one iteration to the next. At high temperatures the average step size is large and the probability is high that the new model will be accepted as the "best fit". This allows the inversion to climb out of local minima and search throughout model space, which enhances the likelihood that the global minimum will be found. After a predetermined number of iterations, the temperature is lowered and the inversion continues with more restrictive criteria. Given a sufficient number of iterations at each temperature, the inversion will converge on a global best fit model.

[28] The procedure starts at a random point in model space (mo) and the misfit function (So) for this model is

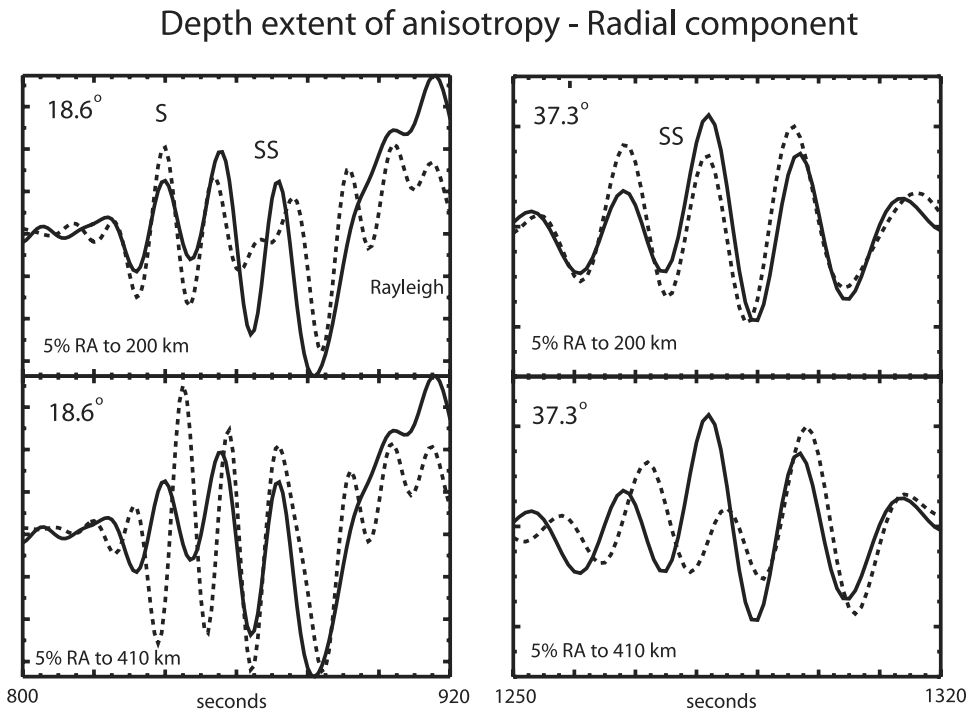

Figure 15. Radial component synthetics for anisotropic models (grey) are compared to data (black) focusing on body wave arrivals. Synthetics were calculated using a constant SH model and anisotropy was calculated relative to that. In the top panels, 5% radial anisotropy is included from the Moho to 200 km depth, with isotropic structure below. In the bottom panels, the anisotropy extends to 410 km.

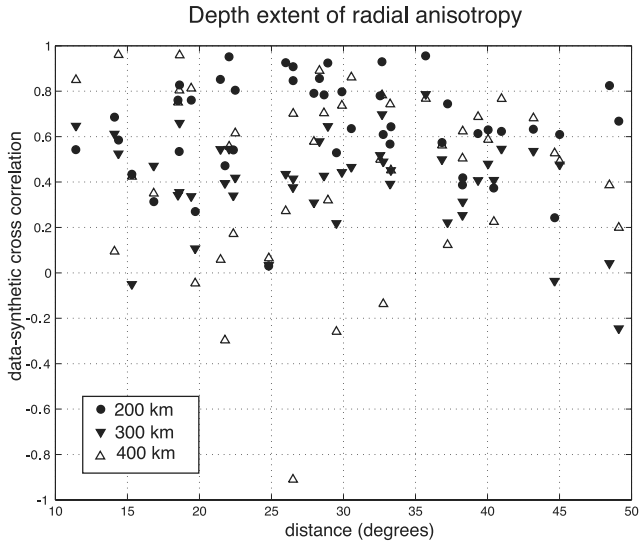

Figure 16. A test of the depth extent of radial anisotropy, focusing on body waves. The cross correlations between radial component data and synthetic seismograms for models with 5% anisotropy extending to 200 km (circles), 300 km (filled triangles) and 400 km (open triangles).

calculated. At each iteration a new model (mnew) is created by taking random steps relative to this initial model until a new "best fit" model is found. The misfit function is recalculated for each new model. The new model is accepted or rejected as an update for mo based on the acceptance criteria. If the misfit is smaller than So the model is automatically accepted. VFSA also allows the possibility for poorer fits to be accepted. This allows the inversion to climb out of local minima and seek a global solution.

[29] Although VFSA is optimized for speed over other random walk methods, it still requires considerably more iterations for convergence than a gradient method does given the same model parameterization. Gradient methods, however, are more restricted in the range of model space that can be explored. Given an arbitrary model, VFSA tends to converge rapidly for the first dozen iterations, but gradually the number of iterations between one model improvement and the next grows larger. For these reasons, we use VFSA at the start of each frequency step and allow it to run for $\sim$100 iterations, then we switch to a CG inversion using the VFSA best fit model as a starting point. This allows the inversion to find a good first order model before the CG procedure starts and prevents the gradient technique from getting caught in a local minimum.

6. The Conjugate Gradient Inversion Method (CG)

[30] Conjugate gradient inversion (CG) is a local descent method that is very effective in large nonlinear inverse problems [*Mora*, 1988; *Tarantola*, 1984]. Gradient methods work by establishing the best 'next step' for the inversion. This is determined by calculating differentials of the misfit function for each model parameter and combining them to establish the vector in model space that points to the smallest value of S. This is the steepest descent direction. Conjugate directions are combinations of the current and previous steepest descent directions and help to speed convergence.

[31] The nonlinear conjugate-gradient inversion method will converge to the best fit solution as long as the starting model is within the valley of the global minimum [*Gauthier et al.*, 1986]. Otherwise the model will either converge to a local minimum, or convergence will be slow. Unlike the VFSA method, the inversion cannot start at a random point in model space. Typically this means that the very long wavelengths of the model parameters must be present in the initial model [*Pica et. al.*, 1990]. To address this problem, we begin by inverting the low frequency structure first using the VFSA method and use this as the initial model for the CG technique.

[32] The CG routine uses differential synthetic seismograms to guide the search through model space. A differential synthetic is a measure of how a small perturbation in a model affects the resulting synthetic seismogram. The simplest way to calculate the differentials is to create synthetics for an initial model, create synthetics for a small

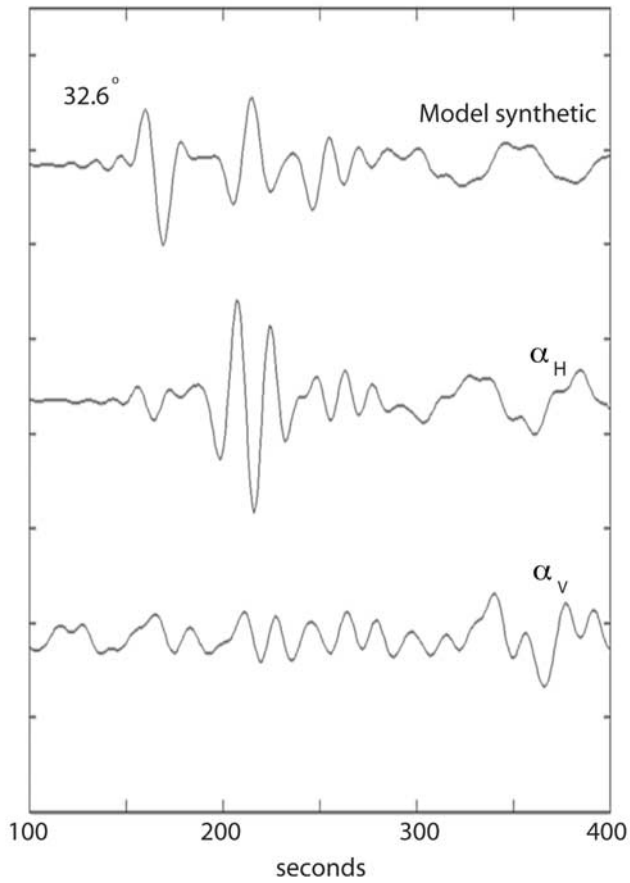

Figure 17. Sensitivity to P anisotropy: Vertical component synthetics and differentials focusing on the P arrival. The top trace is the synthetic for an anisotropic P model ($\alpha V < \alpha H$). The middle and bottom traces are differentials for that model with small perturbations in αH and αV respectively. A large signal is seen in the αH differentials, while very little signal is seen on the αV differentials, indicating that variations in αV have very little effect on the seismograms.

perturbation to that model and subtract on result from the other, although numerical methods have been developed as well [*Randall*, 1994; *Zeng and Anderson*, 1995]. Typically, a separate differential is created for each variable in the inversion. Differential synthetics are very powerful, because they allow the code to determine where the energy on the seismogram comes from, aid in the identification of specific arrivals and allow the inversion to focus in on those that are poorly fit by the current model. An example of differential synthetics is illustrated in Figure 5. The top trace is a full synthetic seismogram for the starting model with major phases identified. The remaining three traces are differentials produced by subtracting synthetics of perturbed models from the original synthetic. In each case the velocity of a single layer has been changed by 0.1% from the original model.

7. Synthetic Test Case

[33] Figure 6 illustrates the ability of the inversion code to model upper mantle seismic waveform data. Synthetic data were created for an isotropic SH velocity model (solid line) and used as the data in an inversion test. A significantly different SH model was used as a starting point in the inversion (dashed line). The dotted line shows the result after 100 VFSA steps. Surface waves dominate the misfit function until the shallowest structure is matched. As the fit to the top of the model improves, the mismatch of the body wave arrivals makes up a more significant percentage of the error function and deeper structure is resolved. The VFSA result was then used as the starting point for the CG inversion which converged on the final model in 7 steps (dashed-dotted line). Note that the inversion result matches most of the major features in the true model including the velocity of the lid and the gradient in the deeper portion of the model. The LVZ is identified, however, the depth is off by ~25 km. This test case used only 2 passes - one each of VFSA and CG, because it was a simple test using noise free synthetic data. Typically, inverting a real data set involves taking a series of passes, alternating between VFSA and CG and gradually increasing the frequency range to minimize the complications of timing uncertainties and noise problems.

[34] One of the consequences of the presence of anisotropy in the lid is that isotropic models of the upper mantle will incorrectly map anisotropic phenomena into variations in seismic velocity structure. To understand how the neglect of anisotropy affects the results of studies assuming isotropy, we performed a series of synthetic tests. Synthetics for an anisotropic model were used as the data in separate isotropic inversions for βSH, βSV and α. We tested a number of cases, varying the size and location of anisotropy in the model and comparing the isotropic inversion results to the horizontal and vertical components of α and β. It is typically possible to match the data perfectly with isotropic models when focusing on a single component (radial, vertical or tangential). When focusing on all components it is not. Figure 7 shows the results of a simple case with α% and β% = 2% down to 220 km. The SH result is very close to the value of βh, although it becomes relatively slower with depth since the phases that travel more deeply are more vertically incident on the anisotropic layer (and thus travel through it more slowly than the shallow phases). The P result is very similar, tracking close to the value of αh. The apparent SV models can differ significantly from βv. The size of the difference is completely dependent on the combination of α% and η. Notice that by comparing the isotropic SV and SH model results we can get a rough estimate of the location and magnitude of anisotropy, although the specifics are not correct. Comparing these models, we also see a small apparent anisotropy extending down into the transition zone.

[35] While the result for an isotropic inversion of anisotropic data is far from the true Earth structure, it can be used as a rough guide to evaluate the presence and magnitude of anisotropy in the data. For an isotropic Earth the SV and SH models should be identical. When the SH and SV results are different, anisotropy is indicated. The isotropic result provides a good estimate of the magnitude and depth extent of anisotropy in the subsurface. This observation can then be used to create an initial model for an anisotropic inversion simultaneously solving for all 3 components of the data.

8. The Procedure

[36] We began by separately inverting each of the 3 components of the data, using an isotropic assumption. Radial and vertical components were inverted for P and SV structure. The tangential component was inverted for SH structure. This was done from low frequency at low radial resolution (~100 km layers) to high frequencies with higher resolution (~25 km layers). The resulting models were compared and the need for anisotropy assessed. Once we had acceptable isotropic models for each of the components of the data, we used those results to create an anisotropic starting model and then inverted the 3-component data simultaneously for both velocity and radial anisotropy. This was again done starting at low frequency and ending at high frequency. In the anisotropic inversion, both seismic velocity and seismic anisotropy were inverted as a function of depth.

[37] Since seismic models are not unique, we repeated the inversion several times at different starting points to get a series of "best fit" model results. Figure 8 illustrates the results for the tangential component (SH) data inversion. The synthetic seismograms for each of these models are virtually indistinguishable at the frequencies used, and each is an equally good fit to the data. The variations between the models provide a sense of the resolution of the data set. The solid line in the figure is the final result. It is a smoothed version of the series of inversion runs produced by averaging. The synthetics from the final result are also an equally good match to the data. Note that the model variations are in the range of <1% for any individual layer and much less overall, and that the basic structure, such as the location of the low velocity zone, are consistent in all the results.

9. The Model

[38] The crustal structure for the East European platform is taken as a multiple layer structure based on the CRUST5.1 model [*Mooney et al.*, 1998] extending to a depth of 41 km. The seismic structure below the crust down to 410 km depth was determined using three-component

waveforms of body and surface wave arrivals from events located on the southern border of the craton. While the sources were located outside the platform, most of the source-receiver path length of each seismogram is within it and the final model should be a good estimate of the average upper mantle seismic structure for the craton. The fundamental mode surface wave data provide excellent resolution of the seismic structure down to ~150 km and body wave arrivals were used to constrain the velocity model below that. Our data is very sensitive to shear structure including shear anisotropy and to the horizontal component of P velocity (αH). η and αV are less well resolved by this data set.

[39] The starting and final models are shown in Figure 9. The initial model was a simple isotropic model with uniform P and S velocity from the Moho to 100 km depth. The final model is a radially anisotropic model with a distinct upper mantle lid over a LVZ (Table 1). A significant improvement in the SH, SV and P data-synthetic match is seen along virtually all the source-receiver paths. This is illustrated by comparing the cross-correlation for the full waveform data of each seismogram for both the initial and final models (Figure 10). The model is characterized by a radially anisotropic seismic lid extending to a depth of 200 km with a largely isotropic mantle below. P structure mimics the SH velocity structure with a high velocity lid extending to 200 km, a drop in seismic velocity followed by a positive velocity gradient down to 410 km. Our model has a positive velocity gradient from 41 km to 100 km depth, and a relatively uniform velocity structure from 100 km to 200 km depth with high SH and PH velocities (4.77 km/s, 8.45 km/s). βH from 41 km to 200 km is uniformly 5% faster than βV. From 200 to 250 km βH drops to 4.70 km/s combined with a reduction in the shear anisotropy to 2%. Note that the mean shear velocity ((βH + βV)/2), is uniform (4.65 km/s) from 100 to 250 km depth and that the structure at the base of the lid is due to a reduction in the shear anisotropy below 200 km. Below 250 km the mantle is largely isotropic (<1% shear anisotropy) with a positive velocity gradient down to 410 km.

10. Resolution Tests

[40] In order to properly interpret our model we wish to determine how well resolved our final model is. In particular, how well constrained is the location and magnitude of anisotropy? Is there definite evidence for a LVZ underlying a fast mantle lid and how well constrained is the lid thickness? To answer these questions we performed a series of resolution tests on our final model, comparing the individual cross-correlation fits for each of our seismograms to determine whether different perturbations to the model might improve the fit along certain paths. Figures 11 and 12 illustrate the sensitivity of the data to the shear velocity in the lid. We tested models in which the high velocity SH lid extends between 100 and 300 km deep. As shown in Figure 11, the fundamental mode Love waves are highly sensitive to structure down to ~200 km and indicate that the lid must extend at least that deeply in order to match the majority of the data. A few traces, particularly at source-receiver offsets under 15° show marginally better fits for thinner lids, probably because they incorporate more of the younger tectonic structures along their path lengths. In order to resolve the deeper structure we focus in on the body wave arrivals (S, SS) (Figure 12). Here we've plotted correlations for models with a 4.77 km/s lid extending to 200, 250, and 300 km. Paths >25° long have the best resolution because the SS arrivals begin to emerge and can be used as a tighter constraint on the model structure. Again, a model with a 200 km thick lid overlying a LVZ gives the best overall results, and the fits for models with lids extending below 250 km become conspicuously poorer.

[41] Shear anisotropy was evaluated by comparing the data to radial and vertical component synthetics for the final model and perturbations from it. We tested both the depth extent and the magnitude of radial anisotropy in the platform. For these tests we kept the SH velocity fixed and made varied SV with respect to that. Figure 13 compares Rayleigh waveform data to synthetics for models with an isotropic, 3%, 5% and 7% uniform anisotropy extending throughout the lid to 200 km. Notice the dramatic differences in the fit of the fundamental mode Rayleigh waves. The Love wave synthetics for each of these models (not shown) are nearly identical so the difference between the isotropic Rayleigh wave synthetic and the data (top of the figure) is equivalent to the Love-Rayleigh mismatch. Note that the higher mode body wave arrivals are also affected by the presence of anisotropy. We determined that models with a uniform 5% radial anisotropy provide the best data-synthetic matches, although models with anisotropic structures varying between 4% and 6% could not be excluded.

[42] In addition to the magnitude of the anisotropy present, we also wanted to determine the location and extent of the anisotropic layer. The observed delays in the fundamental mode Rayleigh wave dictate that anisotropy must be present down to 200 km and perhaps deeper. In Figure 14, we compare the radial component data-synthetic cross-correlation for 3 models: an isotropic model, a model with anisotropy extending to 100 km depth and our best fit model with anisotropy extending to 200 km depth. The full waveform from the direct S arrival through the fundamental mode Rayleigh wave were included in the correlation window. The results show strong evidence that radial anisotropy extends to at least 200 km depth - equivalent to depth of our high SH velocity mantle lid. We focus on the body wave arrivals to determine whether anisotropy extends deeper than that. In Figure 15, two radial component seismic traces are compared to synthetics for models with 0% and 5% anisotropy below 200 km. Notice that a delay of several seconds can occur if significant anisotropy is present. By comparing the results for all of the data (Figure 16), we conclude that there is little anisotropy (<1%) below the seismic lid. Note in that in the figure there is significant scatter in the correlations from trace to trace. This is in part due to the amount of noise present in the data as well as the fact that the arrivals we are looking at have relatively small amplitudes. Some individual traces appear to be better fit by models with significant anisotropy down to 400 km, but this is often caused by the delay time matching up with trailing phases. Overall the model with anisotropy confined to the mantle lid gives the best fit result.

[43] In contrast to our resolution of S anisotropy, P anisotropy is difficult to resolve. Unlike shear anisotropy, a large number of paths, covering a wide range of incidence

angles is typically required to discriminate between αh and αv. These paths will necessarily sample different structure and a different range of depths and there will always be a tradeoff between anisotropic structure and radial structure in the final model. *Anderson and Dziewonski* [1982] showed that Rayleigh waves are sensitive to P anisotropy and η, however Rayleigh waves are much more sensitive to βV and any errors in that measurement could be mapped into the P result. Furthermore, the effect of an increase in P anisotropy on the SV arrivals is identical to that of a decrease in parameter η, and neither are individually resolvable.

[44] We tested the sensitivity of our data to P anisotropy by calculating differential synthetic seismograms for the final P model (Figure 17). A large signal is seen in the αH differentials, while very little signal is seen on the αV differentials, indicating that variations in αV have very little effect on the seismograms. The synthetics for an isotropic P model are virtually identical to the synthetics for an anisotropic P model if αH equals α in the isotropic model. The similarity of these seismograms together with the results of the differential tests indicates that our P data are most sensitive to the horizontal component of P anisotropy.

[45] On the basis of our resolution tests we believe we can make the following conclusions. Isotropic models do not fit the data, the synthetic Rayleigh waves arrive much too early compared to the data. The best overall fit is for a model with 5% shear anisotropy uniformly distributed from 41 km to 200 km and a layer from 200–250 km with 2% anisotropy.

11. Comparison With Other Cratonic Models

[46] One of our objectives is to compare our results for the East European platform to seismic models of other cratons to evaluate features common to all of them. Our results for the East European platform agree very closely with studies of the Australian [*Gaherty et al.*, 1999; *Simons et al.*, 1999], Kaapvaal [*Jordan et al.*, 1999; *Priestley*, 1999; *Qiu et al.*, 1996], Tanzanian [*Ritsema et al.*, 1998], Antarctic [*Roult et al.*, 1994] and Canadian [*Bostock*, 1997; *Grand and Helmberger*, 1984] cratons and with the average seismic structure of Precambrian cratons [*Ekstrom and Dziewonski*, 1998]. Each of these models is characterized by a high velocity seismic lid extending down to between 200 and 250 km depth, coincident with the location of maximum lateral heterogeneity seen in global models of the mantle. This depth also appears to be the base of the petrological lithosphere based on studies of mantle xenoliths. *Kopylova et al.* [1998], for example, identified a depth of 190 km as the base of the petrological lithosphere beneath the Slave craton in Canada based on the apparent source region for both porphyroclastic peridotite and other texturally unequilibrated magmatic rocks. This is consistent with a major seismic discontinuity beneath the Slave craton identified at 195 km depth by *Bostock* [1997].

[47] Anisotropy also appears to be a characteristic of the seismic lid. Our final model includes a uniform 5% shear anisotropy in the mantle lid down to 200 km. No significant variation in the magnitude or gradient of anisotropy is present throughout the lid except at the very base of the lid 200–250 km. Below 250 km no measurable amount of anisotropy (<1%) is present. Similarly both the Australian and Kaapvaal cratons were found to have a uniform 4–5% shear anisotropy in the lid extending to 250 km depth with a sharp transition to an isotropic mantle regime below that [*Gaherty et al.*, 1999; *Simons et al.*, 1999; *Jordan et al.*, 1999]. Significantly, however, the results of the NARS profile through the east European continent identified large shear anisotropy (7%) beneath the Mediterranean, but no clear pattern in shear anisotropy beneath the EEP [*Muyzert et al.*, 1999].

[48] The similarity of the velocity structure, lid thickness, and distribution of anisotropy of these cratonic models points to a common mechanism for the formation and evolution of continental cratons globally. Our results support the conclusions of *Gaherty and Jordan* [1995] that 200 km beneath cratons is either an interface between an anisotropic lithosphere and a more dynamically active regime or is the location of a change in deformation from dislocation to diffusion creep [*Karato*, 1992]. The Pn waveguide model [*Ryberg et al.*, 1995] consisting of horizontally elongated scatterers could also produce anisotropic wave propagation, but their limit of 100 km as the maximum depth of the waveguide is too thin to account for all our observations.

12. Conclusions

[49] The East European platform is underlain by a radially anisotropic seismic mantle lid extending to a depth of 200 km with a largely isotropic mantle below. The model has a positive velocity gradient from 41 km to 100 km depth, and a relatively uniform velocity structure from 100 km to 200 km depth with high SH and PH velocities (4.77 km/s, 8.45 km/s). Shear anisotropy is uniform at 5% ($\beta H > \beta V$) from 41 to 200 km depth, drops to 2% from 200 to 250 km and is isotropic below that. The average shear velocity from 100 to 250 km is also uniform at 4.65 km/s and the drop in anisotropy is matched by a drop in βH to 4.70 km/s combined with an increase in βV to 4.60 km/s. Below 250 km there is a positive velocity gradient in both P and S velocity down to 410 km. P anisotropy is not well resolved, but P structure mimics the SH velocity structure, suggesting that P is also anisotropic within the lid.

References

Anderson, D. L. (1989), *Theory of the Earth*, Blackwell, Malden, Mass.

Anderson, D. L. (1995), Lithosphere, asthenosphere and perisphere, *Rev. Geophys.*, *33*(1), 125–149.

Anderson, D. L., and A. M. Dziewonski (1982), Upper mantle anisotropy—evidence from free oscillations, *Geophys. J. R. Astron. Soc.*, *69*, 383–404.

Artyushkov, E. V. (1984), On the origin of the seismic anisotropy of the lithosphere, *Geophys. J. R. Astron. Soc.*, *76*, 173–178.

Backus, G. E. (1962), Long-wave elastic anisotropy produced by horizontal layering, *J. Geophys. Res.*, *67*, 4427–4440.

Bostock, M. G. (1997), Anisotropic upper-mantle stratigraphy and architecture of the Slave craton, *Nature*, *390*, 392–395.

Ekstrom, G., and A. M. Dziewonski (1998), The unique anisotropy of the Pacific upper mantle, *Nature*, *394*, 168–172.

Forsyth, D. W. (1975), The early structural evolution and anisotropy of the oceanic upper mantle, *Geophys. J. R. Astron. Soc.*, *43*, 103–162.

Fuchs, K., and G. Muller (1971), Computation of synthetic seismograms with the reflectivity method and comparison with observations, *Geophys. J. R. Astron. Soc.*, *23*, 417–433.

Gaherty, J. B., and T. H. Jordan (1995), Lehmann discontinuity as the base of an anisotropic layer beneath continents, *Science*, *268*, 1468–1471.

Gaherty, J. B., M. Kato, and T. H. Jordan (1999), Seismological structure of the upper mantle: A regional comparison of seismic layering, *Phys. Earth Planet. Inter.*, *110*, 21–41.

Gauthier, O., J. Virieux, and A. Tarantola (1986), Two-dimensional nonlinear inversion of seismic waveforms: Numerical results, *Geophysics*, *51*(7), 1387–1403.
Given, J. W., and D. V. Helmberger (1980), Upper Mantle Structure of Northwestern Eurasia, *J. Geophys. Res.*, *85*, 7183–7194.
Glebovitsky, V. A. (1997), *The Early Precambrian of Russia*, Harwood Acad., New York.
Grand, S. P., and D. V. Helmberger (1984), Upper mantle shear structure of North America, *Geophys. J. R. Astron. Soc.*, *76*, 399–438.
Hess, H. H. (1964), Seismic anisotropy of the uppermost mantle under oceans, *Nature*, *203*, 631–669.
Jordan, T. H. (1988), Structure and formation of the continental tectosphere, *J. Petrol.*, *29*, 11–37.
Jordan, T. H., R. L. Saltzer, and J. B. Gaherty (1999), Small-scale anisotropic heterogeneity in the continental upper mantle, *Seismol. Res. Lett.*, *70*(2), 259–260.
Karato, S. (1992), On the Lehmann discontinuity, *Geophys. Res. Lett.*, *19*, 2255–2258.
Kern, H. (1993), P and S wave anisotropy and shear wave splitting at pressure and temperature in possible mantle rocks and their relationship to the rock fabric, *Phys. Earth Planet. Inter.*, *87*, 245–256.
Kopylova, M. G., J. K. Russell, and H. Cookenboo (1998), Upper mantle stratigraphy of the Slave craton, Canada: Insights into a new kimberlite province, *Geology*, *26*(4), 315–318.
Laske, G., and G. Masters (1998), Surface-wave polarization data and global anisotropic structure, *Geophys. J. Int.*, *132*(3), 508–520.
Leeds, A. R. (1975), Lithospheric thickness in the western Pacific, *Phys. Earth Planet. Inter.*, *11*, 61–64.
LeFevre, L. V., and D. V. Helmberger (1989), Upper mantle P velocity structure of the Canadian shield, *J. Geophys. Res.*, *94*, 17,749–17,765.
Li, A., K. M. Fischer, M. E. Wysession, and T. J. Clarke (1998), Mantle discontinuities and temperature under the north American continental keel, *Nature*, *395*, 160–163.
Marquering, H., and R. Snieder (1996), Shear-wave velocity structure beneath Europe, the northeastern Atlantic and western Asia from waveform inversions including surface-wave mode coupling, *Geophys. J. Int.*, *127*, 283–304.
Mechie, J., A. V. Egorkin, K. Fuchs, T. Ryberg, L. Solodilov, and F. Wenzel (1993), P-wave mantle velocity structure beneath northern Eurasia from long-range recordings along the profile QUARTZ, *Phys. Earth Planet. Inter.*, *79*, 269–286.
Montagner, J.-P., and T. Tanimoto (1991), Global upper mantle tomography of anisotropy of seismic velocities and anisotropies, *J. Geophys. Res.*, *96*, 20,337–20,351.
Mooney, W. D., G. Laske, and T. G. Masters (1998), CRUST 5: 1. a global crustal model at 5 degrees X5 degrees, *J. Geophys. Res.*, *103*, 727–747.
Mora, P. (1988), Elastic wave-field inversion of reflection and transmission data, *Geophysics*, *53*(6), 750–759.
Morozova, E. A., I. B. Morozov, S. B. Smithson, and L. N. Solodilov (1999), Heterogeneity of the uppermost mantle beneath Russian Eurasia from the ultra-long-range profile QUARTZ, *J. Geophys. Res.*, *104*, 20,329–20,348.
Muyzert, E., H. Paulssen, and R. Snieder (1999), A seismic cross-section through the east European continent, *Geophys. J. Int.*, *136*, 695–704.
Nicolas, A., and N. I. Christensen (1987), Formation of anisotropy in upper mantle peridotites: A review, *Composition*, *Structure and Dynamics of the Lithosphere-Asthenosphere System*, *Geodyn. Ser.*, vol. 16, edited by K. Fuchs and C. Froidevaux, pp. 111–123, AGU, Washington, D. C.
Nolet, G., J. van Trier, and R. Huisman (1986), A formalism for nonlinear inversion of seismic surface waves, *Geophys. Res. Lett.*, *13*, 26–29.
Paulssen, H. (1987), Lateral heterogeneity of Europe's upper mantle as inferred from modeling of broad-band body waves, *Geophys. J. R. Astron. Soc.*, *91*, 171–199.
Paulssen, H., B. G. Bukchin, A. P. Emelianov, M. Lazarenko, E. Muyzert, R. Snieder, and T. B. Yanovskaya (1999), The NARS-DEEP project, *Tectonophysics*, *313*, 1–8.
Pavlenkova, N. I., and A. V. Yegorkin (1983), Upper mantle heterogeneity in the northern par of Eurasia, *Phys. Earth Planet. Inter.*, *33*, 180–193.
Pavlenkova, N. I., G. A. Pavlenkova, and L. N. Solodilov (1996), High velocities in the uppermost mantle of the Siberian craton, *Tectonophysics*, *262*, 51–65.
Pica, A., J. P. Diet, and A. Tarantola (1990), Nonlinear inversion of seismic reflection data in a laterally invariant medium, *Geophysics*, *55*(3), 284–292.
Priestley, K. (1999), Velocity structure of the continental upper mantle: Evidence from southern Africa, *Lithos*, *48*, 45–56.
Qiu, X., K. Priestley, and D. McKenzie (1996), Average lithospheric structure of southern Africa, *Geophys. J. Int.*, *127*, 558–563.
Randall, G. E. (1994), Efficient calculation of complete differential seismograms for laterally homogeneous earth models, *Geophys. J. Int.*, *118*, 245–254.
Regan, J., and D. J. Anderson (1984), Anisotropic models of the upper mantle, *Phys. Earth Planet. Inter.*, *35*, 227–263.
Ritsema, J., A. A. Nyblade, T. J. Owens, C. A. Langston, and J. C. Van Decar, Upper mantle seismic velocity structure beneath Tanzania, east Africa: Implications for the stability of cratonic lithosphere, *J. Geophys. Res.*, *103*, 21,201–21,213, 1998.
Rodgers, A., and J. Bhattacharyya (2001), Upper mantle shear and compressional velocity structure of the central U.S. craton: Shear wave low-velocity zone and anisotropy, *Geophys. Res. Lett.*, *28*, 383–386.
Roult, G., D. Rouland, and J. P. Montagner (1994), Antarctica II: Upper-mantle structure from velocities and anisotropy, *Phys. Earth Planet. Inter.*, *84*, 33–57.
Rumpker, G., A. Tommasi, and J.-M Kendall (1999), Numerical simulations of depth-dependent anisotropy and frequency-dependent wave propagation effects, *J. Geophys. Res.*, *104*, 23,141–23,153.
Ryberg, T., K. Fuchs, A. V. Egorkin, and L. Solodilov (1995), Observations of high frequency teleseismic Pn on the long-range Quartz profile across northern Eurasia, *J. Geophys. Res.*, *100*, 18,151–18,163.
Ryberg, T., F. Wenzel, A. V. Egorkin, and L. Solodilov (1998), Properties of the mantle transition zone in northern Eurasia, *J. Geophys. Res.*, *103*, 811–822.
Saltzer, R. L., J. B. Gaherty, and T. H. Jordan (2000), How are vertical shear wave splitting measurements affected by variations in the orientation of azimuthal anisotropy and depth?, *Geophys. J. Int.*, *141*, 374–390.
Sen, M., and P. L. Stoffa (1995), *Global Optimization Methods in Geophysical Inversion*, Elsevier Sci., New York.
Simons, F. J., A. Zielhuis, and R. D. van der Hilst (1999), The deep structure of the Australian continent from surface wave tomography, *Lithos*, *48*, 17–43.
Simons, F. J., R. D. van der Hilst, J. P. Montagner, and A. Zielhuis (2002), Multimode Rayleigh wave inversion for heterogeneity and azimuthal anisotropy of the Australian upper mantle, *Geophys. J. Int.*, *151*, 738–754.
Tarantola, A. (1984), Linearized inversion of seismic reflection data, *Geophys. Prospect.*, *32*, 998–1015.
Vinnik, L. P., and V. Z. Ryaboy (1981), Deep structure of the East European platform according to seismic data, *Phys. Earth Planet. Inter.*, *25*, 27–37.
Vinnik, L. P., R. W. E. Green, L. O. Nicolaysen, G. L. Kosarev, and N. V. Petersen (1996), Deep seismic structure of the Kaapvaal craton, *Tectonophysics*, *262*, 67–75.
Walck, M. C. (1984), The P-wave upper mantle structure beneath an active spreading center: The Gulf of California, *Geophys. J. R. Astron. Soc.*, *76*, 697–723.
Xu, Y., and D. Wiens (1997), Upper mantle structure of the southwest Pacific from regional waveform inversion, *J. Geophys. Res.*, *102*, 27,439–27,451.
Zeng, Y. H., and J. G. Anderson (1995), A method for direct computation of the differential seismogram with respect to the velocity change in a layered elastic solid, *Bull. Seismol. Soc. Am.*, *85*(1), 300–307.
Zhao, L. S., and D. V. Helmberger (1993), Upper mantle compressional velocity structure beneath the northwest Atlantic Ocean, *J. Geophys. Res.*, *98*, 14,185–14,196.
Zhao, M., C. A. Langston, A. A. Nyblade, and T. J. Owens (1999), Upper mantle velocity structure beneath southern Africa from modeling regional seismic data, *J. Geophys. Res.*, *104*, 4793–4794.
Zielhuis, A., and G. Nolet (1994), Shear-wave velocity variations in the upper mantle beneath central Europe, *Geophys. J. Int.*, *117*, 695–715.
Zonenshain, L. P., M. I. Kuzmin, and L. M. Natapov (1990), *Geology of the USSR: A Plate-Tectonic Synthesis*, *Geodyn. Ser.*, vol. 21, AGU, Washington, D.C.

S. P. Grand, Department of Geological Sciences, University of Texas at Austin, Austin, TX 78712, USA.
E. Matzel, Lawrence Livermore National Lab, Livermore, CA 94550, USA. (matzel@mantle.llnl.gov)